THE GEOLOGICAL SOCIETY OF AMERICA®

Enhanced precipitation in the Gulf of Mexico during the Eocene–Oligocene transition driven by interhemispherical temperature asymmetry

Mingqiu Hou[1], Guangsheng Zhuang[1,†], Brooks B. Ellwood[1], Xiao-lei Liu[2], and Minghao Wu[1]
[1]*Department of Geology and Geophysics, Louisiana State University, Baton Rouge, Louisiana 70803, USA*
[2]*School of Geosciences, University of Oklahoma, Norman, Oklahoma 73019, USA*

ABSTRACT

Studies reveal that the sea-surface temperature (SST) of the Northern Hemisphere decreased at a smaller amplitude than that of the Southern Hemisphere during the Eocene–Oligocene transition (EOT). This interhemispheric temperature asymmetry has been associated with intensified Atlantic Meridional Overturning Circulation (AMOC) that may have driven enhanced precipitation and weathering in low latitudes and the subsequent drawdown of atmospheric carbon dioxide. However, no quantitative constraints on paleo-precipitation have been reported in low latitudes to characterize the AMOC effect across the EOT. Here, we present the results of high-resolution (ca. 6 k.y. per sample) isotopic and biomarker records from the Gulf of Mexico. Reconstructed precipitation using leaf wax carbon isotopes shows an increase of 44% across the EOT (34.1–33.6 Ma), which is accompanied by a secular increase in SST of ~2 °C during the latest Eocene. We attribute the enhanced precipitation in the Gulf of Mexico to the northward shift of the Intertropical Convergence Zone that was driven by an enlarged polar-tropic temperature gradient in the Southern Hemisphere and an invigorated AMOC. Our findings link changes in meridional temperature gradient and large-scale oceanic circulation to the low-latitude terrestrial hydroclimate and provide paleohydrological evidence that supports CO_2-weathering feedback during the EOT "greenhouse" to "icehouse" transition.

INTRODUCTION

The abrupt shift in the global climate at the Eocene–Oligocene (E–O) boundary marks a transition from ice-free "greenhouse" conditions to glacial "icehouse" conditions. The Eocene–Oligocene transition (EOT) occurred ~34 m.y. ago and involved the reduction in atmospheric pCO_2 (Pearson et al., 2009; Pagani et al., 2011), the onset of continental-scale Antarctic glaciation (Coxall et al., 2005), cooling in high latitudes (Liu et al., 2009), and massive biotic extinctions and evolutionary turnover (Wade and Pearson, 2008). Climate simulation and proxy studies have proposed that the decrease in pCO_2 and opening of Southern Ocean gateways have triggered feedback among continental weathering, reorganization in oceanic structure and circulation, and Antarctic glaciation (DeConto et al., 2008; Lear et al., 2008; Pearson et al., 2009; Elsworth et al., 2017).

Although there is a consensus indicating global cooling from the late Eocene to the early Oligocene, the magnitude and timing of cooling appear different between low and high latitudes and between the two hemispheres. Sea-surface temperature (SST) decreases more substantially at higher latitudes relative to low latitudes (Liu et al., 2009; Wade et al., 2012). In addition, the Northern Hemisphere SSTs did not decrease until the onset of the early Oligocene glacial maximum (EOGM), which occurred later than the Southern Hemisphere cooling at the EOT (Cramer et al., 2009; Liu et al., 2018). This interhemispherical SST asymmetry has been linked to changes in oceanic circulation due to Antarctic glaciation and paleogeographic changes (Goldner et al., 2014; Abelson and Erez, 2017; Elsworth et al., 2017; Hutchinson et al., 2019). Benthic foraminifera $\delta^{18}O$ and $\delta^{13}C$ records from the North Atlantic suggest that modern-like Atlantic Meridional Overturning Circulation (AMOC) was either initiated or invigorated during the EOT (Katz et al., 2011; Borrelli et al., 2014; Abelson and Erez, 2017; Coxall et al., 2018). The coupled ocean-atmosphere models hypothesize that the growth of the Antarctic ice sheet during the EOT increased meridional temperature gradients in the oceans and atmosphere, which then enhanced the northward heat transport in Antarctic Intermediate Water and invigorated the formation of North Atlantic Deep Water (Toggweiler and Samuels, 1995; Sijp et al., 2009). Other model simulations suggest that the AMOC strengthened in the late Eocene due to the opening of the Drake Passage (Elsworth et al., 2017) and closure of the Arctic-Atlantic gateway (Vahlenkamp et al., 2018; Hutchinson et al., 2019; Hutchinson et al., 2021). The inception of AMOC enhanced precipitation at low latitudes on continents, which triggered positive feedback between continental weathering and the drawdown of pCO_2 (Elsworth et al., 2017). Climate models and proxy data have suggested a linkage among change in oceanic circulation, low-latitude precipitation, weathering processes, and the consumption of atmospheric CO_2. However, proxy data that characterize the AMOC effects across the EOT in tropical to subtropical regions are lacking.

The Gulf of Mexico is part of the Atlantic Warm Pool, the extension and intensity of which controls heat transport and hydrological conditions in subtropical Gulf Coastal regions (Wang and Enfield, 2001). Multi-proxy studies have shown an ~3 °C cooling within the Gulf of Mexico during the late Eocene and a significant sea-level fall of ~80 m during the EOGM (Katz et al., 2008; Miller et al., 2008; Wade et al., 2012). However, pollen records from the Gulf Coast region suggest gradual cooling and drying from the late Eocene to the early Oligocene with no significant change in hydrology or ecology near the E–O boundary (Oboh-Ikuenobe and Jaramillo, 2003). Coastal regions tend to present a stronger climatic response that mimics the change in the marine realm due to its proximity to the marine moisture source (e.g., Hampshire Basin in the UK; Sheldon et al., 2016) . However, it is difficult to explain the discordant paleoclimatic data between terrestrial and oceanic systems in the Gulf of Mexico (Oboh-Ikuenobe

Guangsheng Zhuang https://orcid.org/0000-0002-7024-1446
[†]Corresponding author: gzhuang@lsu.edu.

GSA Bulletin;
published online 3 February 2022
https://doi.org/10.1130/B36103.1; 6 figures; 1 supplemental file.

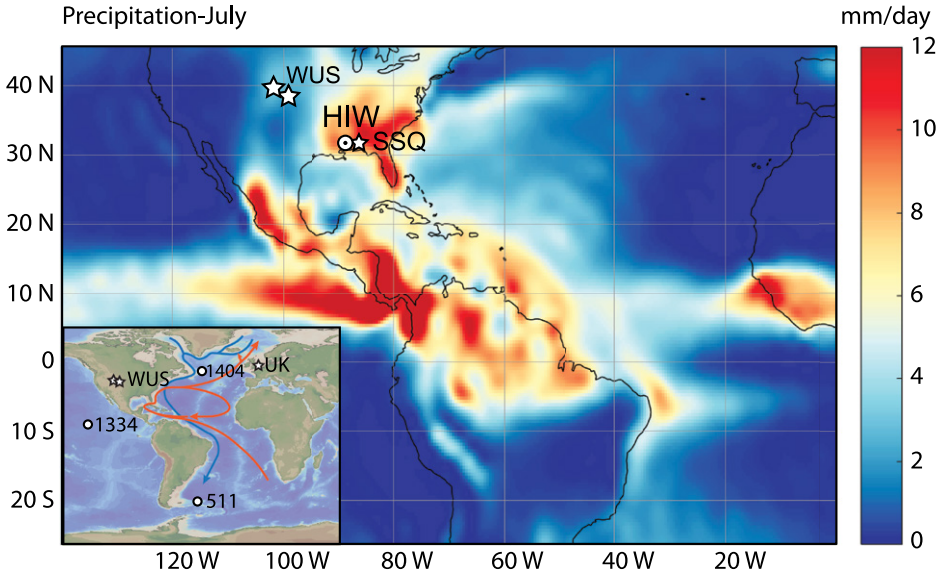

Figure 1. Modern boreal summer precipitation is plotted. The maximum precipitation in the tropics marks the northernmost position of the Atlantic Intertropical Convergence Zone in boreal summer. The Hiwannee (HIW) core site is marked with a circle. Precipitation data (mm/day) are derived from the National Centers for Environmental Prediction/National Center for Atmospheric Research reanalysis data set for the period 1981–2010. Inset shows the locations of sea-surface temperature records (circles) from Integrated Ocean Drilling Program Sites 511 and 1404 (Liu et al., 2009, 2018) and terrestrial paleoclimate records (stars) from the western United States (WUS) (Zanazzi et al., 2007; Fan et al., 2017), St. Stephens Quarry (SSQ) (Katz et al., 2008; Miller et al., 2008; Wade et al., 2012; Houben et al., 2019), and the UK discussed in the text (Hren et al., 2013); blue (deep currents) and orange (surface currents) curves are sketches of Atlantic Meridional Overturning Circulation (AMOC).

and Jaramillo, 2003; Wade et al., 2012). This highlights the necessity for high-resolution paleohydrological reconstruction across the EOT. To fill this gap, we measured carbon ($\delta^{13}C_{wax}$) and hydrogen ($\delta^{2}H_{wax}$) isotopes of terrestrial leaf waxes from a Gulf Coast drill core to quantify the paleohydrology across the EOT. We also measured the tetraether index (TEX_{86}) (Schouten et al., 2002) to reconstruct the SSTs in the Gulf of Mexico. The reconstructed paleoclimate is compared here to contemporaneous terrestrial and oceanic proxy data, which thus makes it possible to understand how the continental hydrology interacted with the change in oceanic and atmospheric systems across the EOT.

LITHOSTRATIGRAPHY, AGE CONSTRAINTS, AND MODERN CLIMATE

Ellwood et al. (2019) used lithostratigraphy, biostratigraphy, geochemical, and geophysical methods to correlate five Eocene–Oligocene boundary successions in the southeastern United States, and these results were compared to the E/O Global Boundary Stratotype Section and Point (GSSP) located near Massignano in central Italy. The Hiwannee core (31.83°N; 88.69°W; Fig. 1) in southeastern Mississippi, USA, is one of the five sites studied. The whole succession is ~60 m in length and extends from the upper Eocene North Twistwood Creek Formation to the lower Oligocene Forest Hill Formation. The Eocene–Oligocene boundary in the study site is placed between the uppermost Eocene Shubuta Clay Member of the Yazoo Formation to the lowermost Oligocene Red Bluff Formation of the Vicksburg Group (Ellwood et al., 2019) (Figs. 2–3). These units were deposited in a shallow marine to marginal marine environmental setting. The Shubuta Clay Member sampled and reported here is ~25 m thick and is composed of greenish, glauconitic clay that grades upward into a bluish, phosphate-rich glauconitic marl. The Red Bluff Formation above is a tan to brownish, glauconitic-rich, marly clay with abundant pyrite-filled burrows. This unit is interbedded with sideritic-carbonate beds that are latterly altered to iron-oxides. Due to variations in bed hardness, the contact between the Red Bluff and the overlying Forest Hill Formations was washed out during the drilling process. Studies of the lithostratigraphy of Eocene–Oligocene units in southeastern Mississippi indicate that the thickness of the Red Bluff Formation is ~3 m (Oboh-Ikuenobe and Jaramillo, 2003). An ~2.5-m-thick succession was recovered in the core, but the uppermost part of the Red Bluff Formation was lost during the drilling process.

The age of the Hiwannee core is constrained by lithostratigraphy, biostratigraphy, and magnetostratigraphy (Ellwood et al., 2019). The Eocene–Oligocene boundary within the Hiwannee core is identified by the last appearance of *Hantkeninidae* in the uppermost Shubuta Clay (Ellwood et al., 2019). Thus, the boundary is placed at the transition from the Shubuta Clay into the base of the Red Bluff Formation. The age model is based on the correlation of magnetic susceptibility data (χ) to the St. Stephens Quarry section (Figs. 2–3), which presents strong 100 k.y. eccentricity cycles that are directly comparable to the GSSP in Italy (Ellwood et al., 2019). The χ data for the Oligocene Red Bluff Formation within the Hiwannee core shows the same 100 k.y. cyclicity as that at the St. Stephens Quarry, while the cyclicity of the upper Eocene Shubuta in the Hiwannee core is twice that in the St. Stephens Quarry sequence (Ellwood et al., 2019) (Fig. 3). We compared the χ data from the Hiwannee core to the data from the St. Stephens Quarry to derive the top (33.45 Ma) and bottom (34.1 Ma) ages of the Hiwannee samples. Ages of Hiwannee core samples within each χ zone were determined using linear interpolation (Fig. 3). In this study, the E–O boundary was placed at 33.8 Ma after comparison with published proxy data, but it should be noted that the latest Geological Time Scale has placed the E–O boundary at 33.9 Ma (Ogg et al., 2016).

The Hiwannee core site, which is situated in the eastern part of the Gulf Coastal Plain, is fed by tropical maritime air masses (Lambert and Aharon, 2010). The study area experienced moderate seasonality; monthly temperatures ranged from ~9 °C to 28 °C, and the average monthly precipitation ranged from ~85 mm (Fall) to ~185 mm (Spring) (www.ncdc.noaa.gov). Convectional rainfall events (hurricanes and tropical storms) are dominant during Summer, while a frontal style weather system driven by westerly jet streams controls Fall, Winter, and Spring precipitation (Lambert and Aharon, 2010). Interannual change in atmospheric circulation has been linked to the El Ninõ–Southern Oscillation and the position of the Bermuda High, which influences moisture transport during the Winter/early Spring and Summer/early Fall seasons, respectively (Katz et al., 2003; Mo and Schemm, 2008; Lambert and Aharon, 2010). Changes in paleoclimate on a glacial–interglacial time-scale have been associated with the shift of the Intertropical Convergence Zone (Suh et al., 2020).

METHODS AND MATERIALS

The Hiwannee core was sampled at 5–10 cm intervals (119 samples) covering ~700 k.y. from

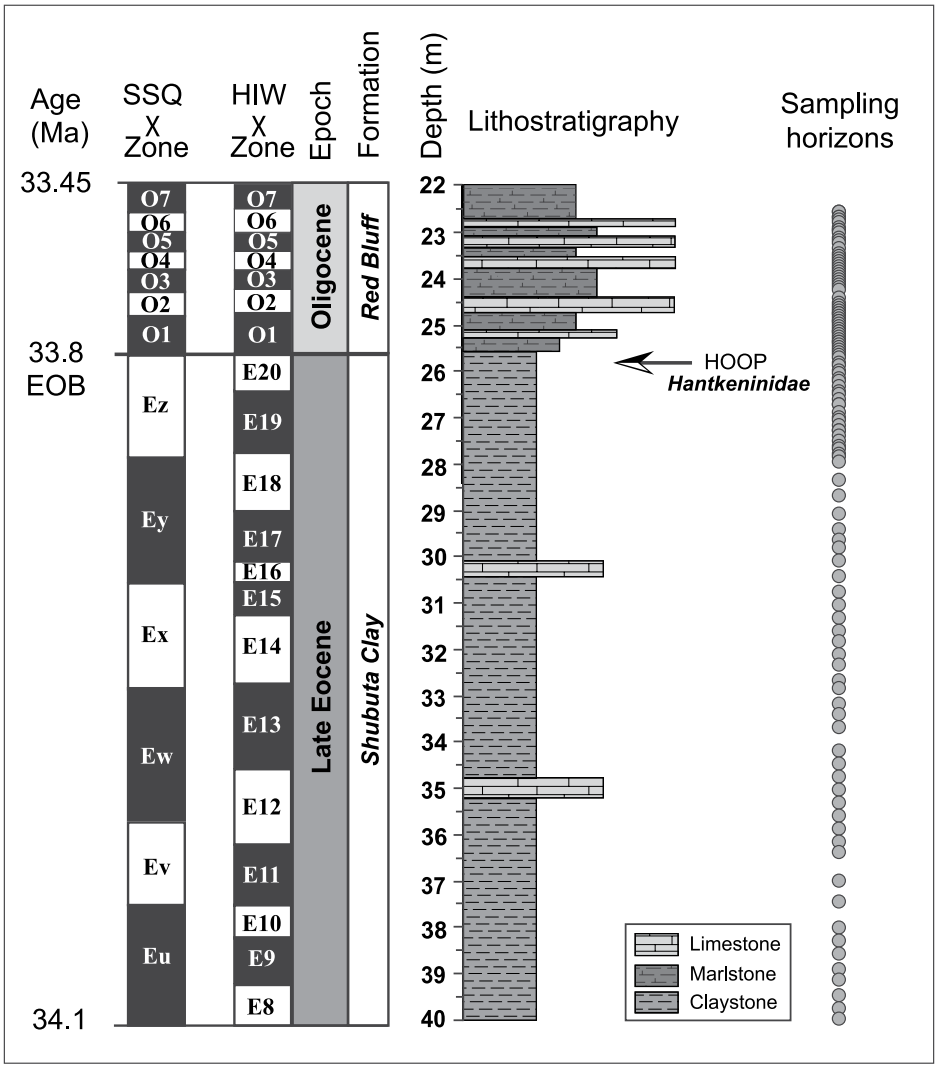

Figure 2. Lithostratigraphy and sampling horizons (gray circles) for the Hiwannee (HIW) core in Mississippi, southeastern United States, are shown. Magnetic susceptibility data, interpretation of chronology, and the highest observed occurrence point (HOOP) of foraminifera *Hantkeninidae* are adapted from Ellwood et al. (2019). SSQ—St. Stephens Quarry; EOB—Eocene–Oligocene boundary. The white versus black boxes in bar logs represent low versus high magnetic susceptibility values.

the uppermost Eocene Shubuta Clay Member to the lowermost Oligocene Red Bluff Formation of the Vicksburg Group (Ellwood et al., 2019). We studied the weighted mean δ^2H_{wax} and $\delta^{13}C_{wax}$ values of long-chain *n*-alkanes (*n*-C_{27}, *n*-C_{29}, and *n*-C_{31}) from the Hiwannee core collected at the town of Hiwannee in Wayne County, southern Mississippi, USA (31.83°N; 88.69°W; Fig. 1). Given that the Antarctic ice sheet rapidly grew during the EOGM, leading to an increase in seawater oxygen and hydrogen values, the δ^2H enrichment, caused by ice sheet growth, was subtracted to generate a record with the ice volume effect removed (δ^2H_{wax-i}). The $\delta^{13}C_{wax}$ data were then used to quantify the change in mean annual precipitation (MAP) across the EOT based on empirical equations generated by a global compilation of modern plants by Diefendorf et al. (2010) and new data for trees in the Gulf Coast region (Table S4[1]). Also measured were the tetraether index (TEX_{86}) values (Schouten et al., 2002) to reconstruct the SSTs of the Gulf of Mexico. The reconstructed hydrology and SST history are compared to contemporaneous terrestrial and oceanic proxy data to address the interaction between the oceanic and atmospheric systems across the EOT.

[1]Supplemental Material. Table S1: Leaf wax isotopic records in the Gulf of Mexico; Table S2: Reconstructions of mean annual precipitation based on leaf wax carbon isotopic records; Table S3: Sea surface temperature reconstructions; Table S4: Leaf wax isotopic records of modern trees. Please visit https://doi.org/10.1130/GSAB.S.17238875 to access the supplemental material, and contact editing@geosociety.org with any questions.

Total Lipid Extraction, Column Chromatography, and Characterization

Samples were ground with a mortar and pestle to a coarse-sand size and freeze-dried for 48 h before extraction. Total lipids were extracted with Soxhlet extractors using the azeotrope of dichloromethane (DCM)/methanol 2:1 (v/v) for 48 h. Total lipid extracts (TLE) were evaporated until dry under a stream of purified nitrogen. Organic compounds in TLE were separated into apolar, intermediate, and polar fractions using a pipette column filled with ~0.5 g of activated silica gel and sequentially eluted with 2 ml hexane, 4 ml DCM, and 4 ml methanol; *n*-Alkanes contained in apolar fractions were re-dissolved into 1500 μL of hexane. *n*-Alkane abundances were then determined using a Thermal Trace 1310 gas chromatography (GC)–flame ionization detector (FID) fitted with a programmable–temperature vaporization (PTV) injector and TG-1MS column (60 m long, 0.25 mm i.d., 0.25 μm film thickness). Samples were carried by helium at a rate of 2 ml/min. GC oven temperature was programmed to ramp from 60 °C (thermal holding for 1 min) to 320 °C at 15 °C/min (holding for 20 min). Individual *n*-alkanes were identified by comparing elution time with a reference standard (Mix A6, *n*-C_{16} to *n*-C_{30}; A. Schimmelmann, Indiana University Bloomington, USA).

Terrestrial vascular plant-produced, long-chain *n*-alkanes are dominated by a homologous series from *n*-C_{25} to *n*-C_{33}, with odd-over-even carbon number predominance (Eglinton and Hamilton, 1967), which is expressed by the carbon preference index (CPI):

$$\mathrm{CPI} = \frac{1}{2}\frac{\sum \mathrm{A}(23-33)\mathrm{odd} + \sum \mathrm{A}(25-35)\mathrm{odd}}{\sum \mathrm{A}(24-34)\mathrm{even}}, \quad (1)$$

where A stands for the areas of individual *n*-alkane compounds, which are calculated by integrating ion trace peaks from a gas chromatograph using the Xcalibur software.

The P_{aq} index (values range from 0 to 1) is used to reflect the relative contribution of leaf wax *n*-alkanes from aquatic macrophytes (*n*-C_{23} and *n*-C_{25}) versus terrestrial vascular plants (*n*-C_{29} and *n*-C_{31}) (Ficken et al., 2000). P_{aq} values were determined using the equation:

$$P_{aq} = \frac{\mathrm{A}(23+25)}{\mathrm{A}(23+25+29+31)}, \quad (2)$$

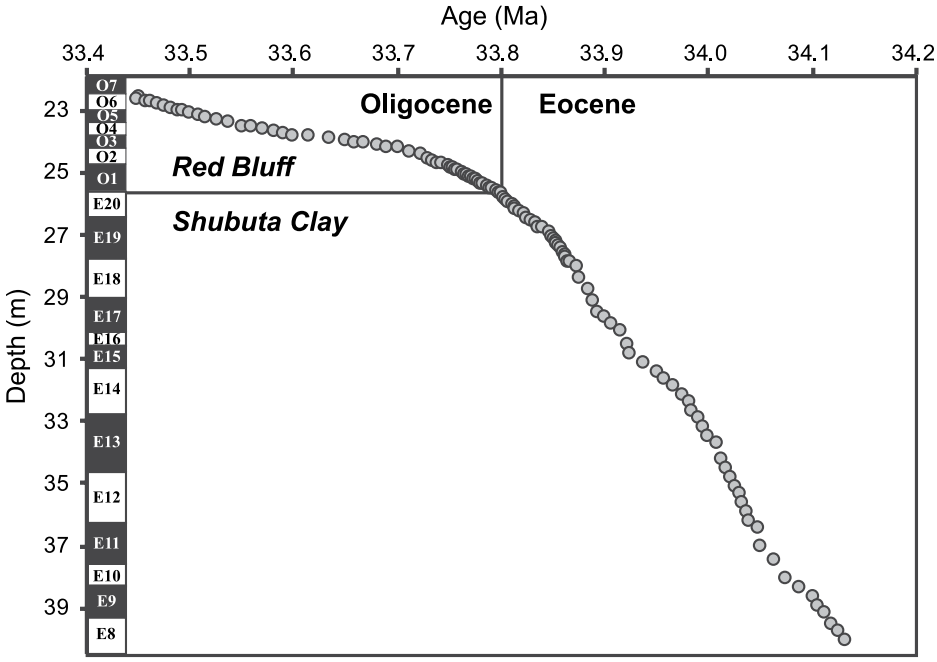

Figure 3. Age-depth relationship is shown for the Hiwannee core from the late Eocene to the early Oligocene. The magnetic susceptibility data are from Ellwood et al. (2019). Gray circles denote the samples.

where A stands for the areas of individual *n*-alkane compounds in chromatography.

Leaf Wax Carbon Isotopic Analysis

Leaf wax carbon isotopic values were measured using a Trace 1310 GC coupled with a Thermo Delta V Advantage isotope ratio mass spectrometer (IRMS) with a Thermo Isolink interface. The Trace 1310 GC was fitted with a PTV injector and a TG-5MS column (30 m long, 0.25 mm i.d., 0.25 μm film thickness). Samples were carried by helium at a rate of 2 ml/min. Compounds were separated by the GC, with the temperature being programmed to ramp up from 60 °C (held for 2 min) to 170 °C at 14 °C/min, to 300 °C at 3 °C/min, and then to 320 °C at 14 °C/min, with an isothermal holding of 5 min. A duplicate analysis was applied to each sample. The *n*-alkane reference materials of Mix A6 were measured every four to six analyses to monitor instrumental drift. The mean analytical precision for $\delta^{13}C$ of Mix A6 is 0.1‰. Carbon isotopic values were calibrated relative to Mix A6 and reported relative to the Vienna Pee Dee Belemnite (VPDB) standard and expressed in per mil (‰):

$$\delta^{13}C = \left(\frac{R_{sample}}{R_{reference}} - 1 \right), \quad (3)$$

where R represents the $^{13}C/^{12}C$ ratios in samples and standard reference. The weighted mean $\delta^{13}C$ values of n-C_{27}, n-C_{29}, and n-C_{31} were calculated as follows:

$$\delta^{13}C_{wax} = \frac{\sum A_i \times \delta^{13}C_i}{\sum A_i}, \quad (4)$$

where A stands for the areas of *n*-alkanes with i (27–31) indicating the carbon chain-length.

Leaf Wax Hydrogen Isotope Analysis

Leaf wax hydrogen isotope values were measured by the same GC-Isolink-IRMS system with a high-temperature conversion (HTC) configuration. GC and column settings were identical to those used in the carbon isotope analysis. The H_3^+ factor was measured three times daily prior to isotopic analysis. A duplicate analysis was applied to each sample with a mean analytical precision of 1.6‰ for δ^2H. The *n*-alkane reference material (Mix A6) was measured every four to six analyses to monitor instrumental drift. Hydrogen isotope ratio values were calibrated relative to Mix A6 and reported relative to the Vienna Standard Mean Ocean Water (VSMOW) standard. The mean analytical precision of δ^2H for Mix A6 is 1‰. Hydrogen isotopic compositions were determined using the following equation and expressed in per mil (‰):

$$\delta^{2}H = \left(\frac{R_{sample}}{R_{reference}} - 1 \right), \quad (5)$$

where R stands for the $^2H/H$ ratios of samples and reference materials. The weighted mean δ^2H values for n-C_{27}, n-C_{29}, and n-C_{31} are calculated as follows:

$$\delta^{2}H_{wax} = \frac{\sum A_i \times \delta^{2}H_i}{\sum A_i}, \quad (6)$$

where A stands for the areas of *n*-alkanes and i (27–31) indicates the carbon chain-length.

Analysis of Glycerol Dialkyl Glycerol Tetraethers

The methanol fraction containing glycerol dialkyl glycerol tetraethers (GDGTs) was analyzed using an Agilent 1290 series ultra-high performance liquid chromatography (UPLC) system that was coupled to an Agilent 6530 qTOF mass spectrometer through an Agilent jet stream dual electrospray ionization (AJS-ESI) interface following the methodology of Liu et al. (2019). The relative abundance of GDGTs is used to derive the TEX_{86} index values that were converted to the SSTs by applying a linear TEX_{86}^H-SST relationship with a calibration error of ± 2.5 °C (Kim et al., 2010). The calibration results are provided in Table S3 (see footnote 1) using a linear relationship as in Schouten et al. (2002) and a Bayesian regression model (BAYSPAR) (Tierney and Tingley, 2014).

REMOVAL OF ICE VOLUME EFFECTS FROM δ^2H_{WAX} RECORDS

The rapid growth of the Antarctic ice sheet during the EOGM (ca. 33.65 Ma) caused the enrichment of δ^2H in seawater and thus influenced leaf wax δ^2H_{wax} values in samples younger than 33.65 Ma. Previous studies of marine $\delta^{18}O$ records reveal a 0.6‰ enrichment in seawater $\delta^{18}O$ due to Antarctic glaciation (Katz et al., 2008; Miller et al., 2008). Therefore, the ice volume effects on the δ^2H_{wax} record are corrected as follows:

(1) The slope of the local meteoric water line (7.2) from the International Atomic Energy Agency (IAEA) station in Alabama (Lambert and Aharon, 2010) was used to convert the change in seawater $\delta^{18}O$ to δ^2H. The change of 0.6‰ in seawater $\delta^{18}O$ is equivalent to a 4.3‰ change in δ^2H. The change in seawater δ^2H is assumed to be reflected in precipitation δ^2H_p.

(2) The relationship between the hydrogen isotopic composition of leaf waxes (δ^2H_{wax}) and precipitation water (δ^2H_p) is defined by the following,

$$\varepsilon_{wax/p} = \frac{\delta^{2}H_{wax} + 1}{\delta^{2}H_{p} + 1} - 1, \quad (7)$$

where $\varepsilon_{wax/p}$ is used to characterize the apparent fractionation between δ^2H_{wax} and δ^2H_p, which is reported in per mil (‰) (Sachse et al., 2012). During the late Eocene and early Oligocene, warm temperate forests were predominant in the southeastern United States (Oboh-Ikuenobe and Jaramillo, 2003), and there was little C_4 grassland before the early Miocene (Tipple and Pagani, 2010). The average $\varepsilon_{wax/p}$ value (~130‰) derived from *n*-C_{29} of North American C_3 forest (Hou et al., 2007) was used here to convert the change in δ^2H_p to the equivalent of 4.9‰ in δ^2H_{wax}.

(3) Then the ice volume-induced δ^2H_{wax} enrichment (4.9‰) was subtracted from samples that are younger than 33.65 Ma to obtain an ice-volume corrected δ^2H_{wax-I} record.

RESULTS

Characterization of *n*-Alkanes

Plant cuticular waxes coating leaf surfaces maintain water balance and prevent physical damage to leaf cells. *n*-Alkanes, as one of the major compounds consisting of leaf waxes, are ubiquitously preserved in almost all types of sedimentary environments. A rigorous cut-off of CPI values for terrestrial higher plant sources has been suggested to be greater than two (Bush and McInerney, 2013). Samples with CPI values near one are suspected to be influenced by thermal alteration or degradation after deposition. Our CPI values range from 2.2 to 4.0, which indicates that Hiwannee sediments are less likely to be influenced by post-depositional alteration.

P_{aq} values are used to evaluate the relative aquatic input relative to that of terrestrial plants, with a higher P_{aq} value indicating a higher proportion of aquatic input. P_{aq} values vary between 0.2 and 0.5 in the whole series, and there is a marked decrease of ~0.2 between ca. 33.75 Ma and ca. 33.65 Ma (Fig. 4A).

Leaf Wax Carbon and Hydrogen Isotopic Results

The $\delta^{13}C_{wax}$ values at Hiwannee decrease by ~1.6‰ across the EOT, with mean value shifts from −29.5‰ during the late Eocene to −31.1‰ after the EOGM (Fig. 4B). This change in $\delta^{13}C_{wax}$ values is synchronous with a positive shift in benthic foraminifera $\delta^{18}O$ records from the global data set (Figs. 4B and 4E). The δ^2H_{wax-I} record shows an ~10‰ negative shift over 350 k.y. (ca. 34.00–33.5 Ma) across the EOT, which is coeval with the negative shift in $\delta^{13}C_{wax}$ values (Figs. 4B−4C). The mean δ^2H_{wax-I} values change from −158‰ before the EOT to −169‰ after the EOGM.

TEX_{86}-Based Sea-Surface Temperature Reconstructions

TEX_{86}-based SST reconstructions in the Hiwannee core (Fig. 4D) increase from 28 °C to 31 °C from 34.1 Ma to 33.8 Ma and decrease by ~3 °C within the following 50 ka (33.8−33.75 Ma). While samples younger than 33.75 Ma show high terrestrial-branched GDGT (br−GDGT) input, multivarious quantitative

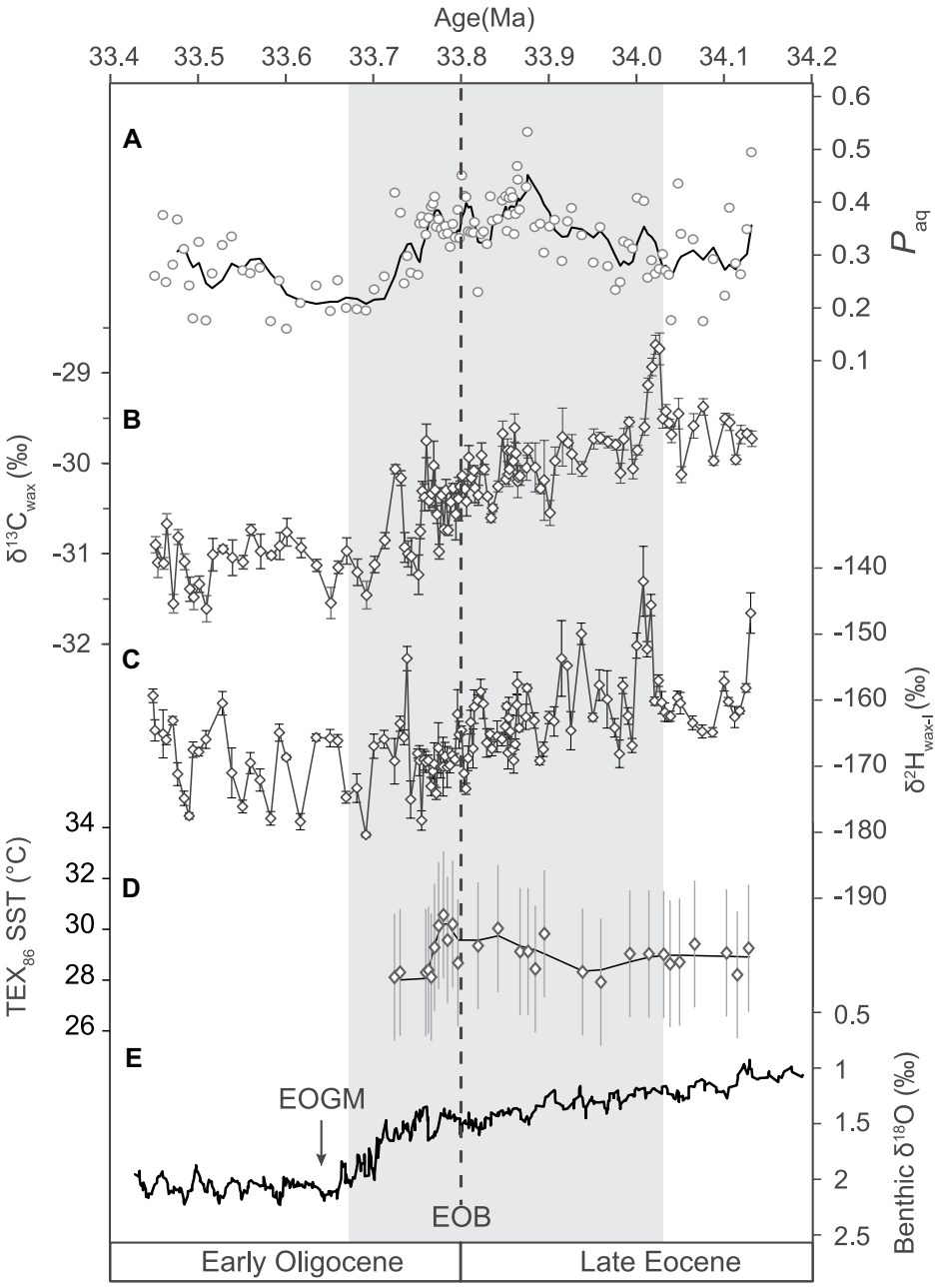

Figure 4. Paleoclimatic reconstruction in the Gulf of Mexico is based on leaf wax carbon and hydrogen isotopes and TEX_{86} sea-surface temperatures (SSTs). (A) P_{aq} record; black curve is generated by Loess regression. (B) $\delta^{13}C_{wax}$ record. (C) δ^2H_{wax-I} record. (D) TEX_{86} SSTs, with branched and isoprenoid tetraethers (BIT) < 0.5 and a calibration error of ± 2.5 °C; black curve is generated by local regression. SSTs with BIT > 0.5 are reported in the Supplementary Material (see footnote 1). (E) A global compilation of benthic $\delta^{18}O$ records with the black line represents a 10-point moving average (Cramer et al., 2009). The shaded bar denotes the Eocene–Oligocene transition (EOT) interval. EOGM—early Oligocene glacial maximum; EOB—Eocene–Oligocene boundary.

and correlation analyses were performed and showed that samples having a branched and isoprenoid tetraethers (BIT) index smaller than 0.5 are best for constraining the SST variations (Supplemental Material; see footnote 1).

DISCUSSION

Evidence of Early Oligocene Glacial Maximum Sea-Level Fall

A drastic change in P_{aq} values (Fig. 4A) is synchronous with the EOGM. P_{aq} values decreased markedly by ~0.2 at ca. 33.65 Ma (Fig. 4A), which indicates an increase in terrestrial organic matter input that may have resulted from rapid eustatic fall driven by Antarctic glaciation. Marine $\delta^{18}O$ and Ca/Mg records from nearby successions in the St. Stephens Quarry site in Alabama support the major drop in sea level in the Gulf of Mexico associated with the EOGM (Katz et al., 2008; Miller et al., 2008).

Hydrological History in the Gulf of Mexico during the Eocene–Oligocene Transition

$\delta^{13}C_{wax}$ is a function of the $\delta^{13}C$ of atmospheric CO_2 ($\delta^{13}C_{atm}$) and photosynthetic fractionation (Δ_{leaf}) during carbon fixation (Farquhar et al., 1982). Photosynthetic fractionation is modulated by both physiological (photosynthetic pathways) and environmental (water stress) variables. Plants with different photosynthetic pathways can result in distinct carbon isotopic signatures. C_3 (Calvin-Benson) carbon fixation pathways show a larger fractionation than the C_4 (Hatch-Slack) pathways (Diefendorf and Freimuth, 2017). Therefore, the mean $\delta^{13}C_{wax}$ value of C_3 plants is ~−33‰, whereas the mean value of C_4 plants is ~−22‰. $\delta^{13}C_{wax}$ data from the Hiwannee site range from −31.6‰ to −28.7‰, which indicates that C_3 plants were dominant in the Gulf Coast region during the late Eocene and into the early Oligocene. The results reported here are comparable to the $\delta^{13}C_{wax}$ records from the Gulf of Mexico during the same time interval (Tipple and Pagani, 2010). Variation of $\delta^{13}C_{wax}$ values in the Hiwannee core reflects a change in Δ_{leaf}, as the $\delta^{13}C_{atm}$ is relatively constant across the EOT, as indicated by benthic foraminifera $\delta^{13}C$ records (Tipple et al., 2010). Water stress predominantly controls Δ_{leaf} by regulating leaf gas exchange via constraints on stomatal conductance. Therefore, plant carbon isotopic fractionation is strongly correlated with mean annual precipitation, so that $\delta^{13}C_{wax}$ values decrease with increasing precipitation (Diefendorf et al., 2010). A 1.6‰ negative shift in $\delta^{13}C_{wax}$ values in Hiwannee implies an increase in precipitation in the Gulf of Mexico through the EOT.

δ^2H_{wax} from modern lake sediments reflects the hydrogen isotopic composition of source waters and varies among plant forms due to biosynthetic differences (Hou et al., 2008; Sachse et al., 2012). As the primary control of δ^2H_{wax} values, precipitation δ^2H_p changes as a function of temperature, precipitation amount, evaporation, and other climatic factors. δ^2H_{wax} has been used to reconstruct the long-term hydrologic evolution of the Great Plains of North America since the late Eocene (Tipple and Pagani, 2010). The current study focuses on the change in paleoclimate in Gulf Coastal areas across the EOT. The variation of interannual precipitation δ^2H_p around the Gulf Coast mainly reflects changes in rainfall amount; lower δ^2H_p values indicate increasing precipitation and vice versa (Lambert and Aharon, 2010). Seasonal and annual temperatures have little influence on precipitation isotopic values ($\delta^{18}O$ and δ^2H) in the U.S. Gulf Coast (Vachon et al., 2010) due to weak seasonality and a single moisture source from tropical maritime air masses (Lambert and Aharon, 2010), so that isotopic amount effects may overwrite the temperature effects. Long-term temperature changes are unlikely to cause observed negative shifts in δ^2H_{wax-I} values because TEX_{86}-based SSTs slightly increase from 34.1 Ma to 33.8 Ma, which is supposed to increase rather than decrease δ^2H_{wax-I} values due to the effects of isotopic temperature (Rozanski et al., 1993). Moreover, the decrease in hydrogen isotope values is less likely attributed to the reduced vapor content in air and the sub-cloud evaporation associated with cooling because the climate in the Gulf of Mexico was warmer during this interval (Figs. 4C–4D). Therefore, the negative shift in δ^2H_{wax-I} across the EOT represents an increase in the amount of precipitation.

Change in plant communities should have a negligible effect on $\delta^{13}C_{wax}$ and δ^2H_{wax-I} values in the Hiwannee core across the EOT. Studies conducted using modern plants suggest that plant carbon and hydrogen isotopes vary among taxonomic groups (Diefendorf et al., 2010; Sachse et al., 2012). For example, carbon isotopic fractionation of gymnosperms is ~3–5‰ less than that of angiosperms, which results in higher $\delta^{13}C_{wax}$ values in conifers than in angiosperms (Diefendorf et al., 2011). Hydrogen isotopic fractionation in graminoids is greater than in trees and shrubs by ~30‰ (Sachse et al., 2012). The Gulf Coast region was dominated by tropical to subtropical forest assemblages during the late Eocene and the early Oligocene, including *Quercoidites*, *Sequoiapollenits*, *Cupressacites*, and *Cyrillaceaepollenites* (Oboh-Ikuenobe and Jaramillo, 2003). Although *Quercoidites* increase slightly during the Oligocene, there is no significant paleofloristic change and turnover across the Eocene–Oligocene boundary (Oboh-Ikuenobe and Jaramillo, 2003).

$\delta^{13}C_{WAX}$-BASED RECONSTRUCTIONS OF PRECIPITATION

$\delta^{13}C_{wax}$ records were used to reconstruct EOT precipitation in the Hiwannee. The change in precipitation is calculated relative to the mean annual precipitation during the latest Eocene (prior to 34.0 Ma). The reconstruction of precipitation using $\delta^{13}C_{wax}$ is based on empirical relationships of modern leaf discrimination (Δ_{leaf}) values as a function of mean annual precipitation (Diefendorf et al., 2010). Conversion from $\delta^{13}C_{wax}$ to Δ_{leaf} involves two processes: (1) determination of Δ_{leaf} between $\delta^{13}C$ of the bulk leaf ($\delta^{13}C_{leaf}$) and $\delta^{13}C$ of the atmosphere ($\delta^{13}C_{atm}$) and (2) calculation of biosynthetic fractionation (ε_{leaf}) between $\delta^{13}C_{leaf}$ and $\delta^{13}C_{wax}$, expressed by:

$$\Delta_{leaf} = \left(\frac{\delta^{13}C_{atm}+1}{\delta^{13}C_{leaf}+1}-1\right)\times 10^3, \quad (8)$$

$$\varepsilon_{leaf} = \left(\frac{\delta^{13}C_{wax}+1}{\delta^{13}C_{leaf}+1}-1\right)\times 10^3, \quad (9)$$

where $\delta^{13}C_{atm}$ is ~−5.9‰ during this interval (Tipple et al., 2010). $\delta^{13}C_{leaf}$ is the carbon isotopic composition of the bulk leaf. The ε_{leaf} between $\delta^{13}C_{wax}$ of long-chain *n*-alkanes (*n*-C_{27}, *n*-C_{29}, and *n*-C_{31}) and bulk leaf $\delta^{13}C_{leaf}$ is ~-4.6‰ for C_3 plants based on the compilation of modern plants (Tipple and Pagani, 2010; Diefendorf and Freimuth, 2017). Analysis of woody C_3 plants from the global data set indicates that Δ_{leaf} is linearly correlated with the log of mean annual precipitation (MAP) (Diefendorf et al., 2010). To quantify the change of MAP in the Hiwannee core through the EOT, we calculated the Δ_{leaf} for our $\delta^{13}C_{wax}$ records and then employed an empirical Δ_{leaf} – MAP relationship, expressed by:

$$\log(\mathrm{MAP}) = 0.10(\pm 0.04) \times \Delta_{leaf} + 1.01(\pm 0.08)\,(\mathrm{R} = 0.73,\ \mathrm{n} = 105). \quad (10)$$

Data used to derive Equation (10) are from a global compilation of modern plants by Diefendorf et al. (2010) and new data for trees in the Gulf Coast region (Fig. 5; Table S4; see footnote 1). Pollen data indicate a stable plant assemblage in Gulf Coast regions. Hence, we

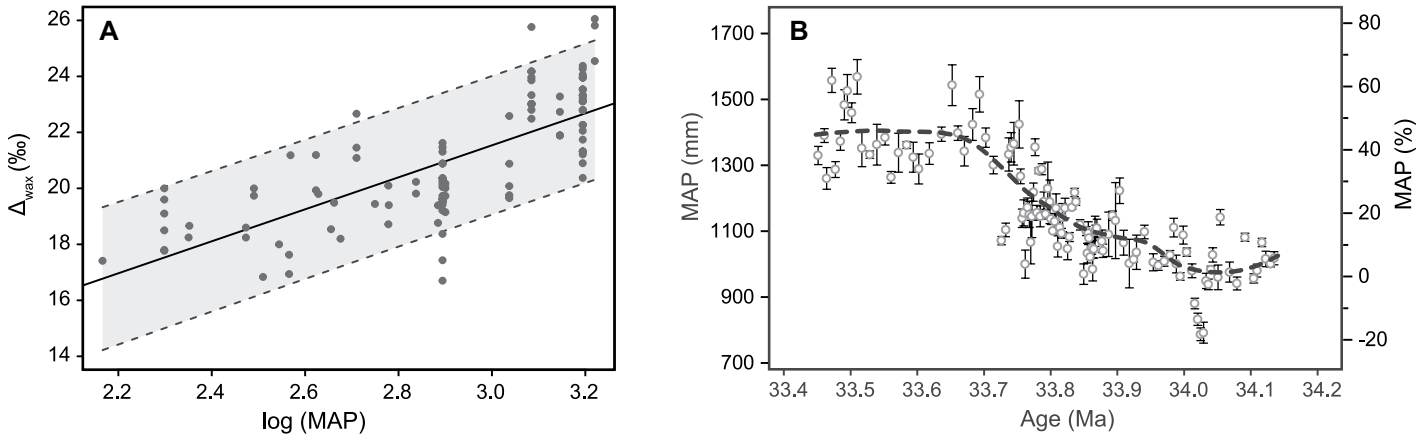

Figure 5. Mean annual precipitation (MAP) reconstruction is based on Δ_{leaf}. (A) The linear relationship between Δ_{wax} and log(MAP), with MAP data in millimeters. The Δ_{leaf} and MAP data (dots) are adapted from Diefendorf et al. (2010). The shaded area denotes the 90% confidence interval. (B) Change of mean annual precipitation (MAP) in millimeters (left vertical axis) and in percentage (right vertical axis) at Hiwannee across the Eocene–Oligocene transition is quantified by the $\delta^{13}C_{wax}$ record. The data are presented in dots with dashed line generated by local regression. MAP% are calculated relative to the mean values for the late Eocene (before 34.0 Ma) and are reported in percentage (%).

argue that $\delta^{13}C_{wax}$ values in the Hiwannee core are reliable for predicting precipitation change across the EOT. $\delta^{13}C_{wax}$-based reconstructions of precipitation amount increase from an average of 965 ± 30 mm during the latest Eocene (before 34.0 Ma) to 1392 ± 37 mm during the early Oligocene (33.45–33.70 Ma) (Fig. 5), which is equivalent to an increase of 44% in precipitation across the EOT. Genetic variability among plant species may impact the absolute values of the predicted MAP (Ehleringer et al., 1991; Diefendorf and Freimuth, 2017). However, if this empirical relationship is valid for individual plant species and the composition of plant communities is stable, the uncertainty of reconstruction is likely to affect the absolute precipitation amount but not the proportional change in MAP (MAP%).

Interhemispheric Temperature Asymmetry across the Eocene–Oligocene Transition

Our TEX_{86}-based SST reconstructions show a cooling magnitude (~2–4 °C) similar to that of the record at the St. Stephens Quarry (Wade et al., 2012) across the EOT. The new SSTs reported here also capture a secular warming trend within ~300 k.y. before this cooling, which is concordant with an increasing SST in the Gulf of Mexico and equatorial Atlantic during the late Eocene (Tremblin et al., 2016; Houben et al., 2019). Warming at low latitudes during the late Eocene might have reflected increasing heat accumulation in the tropical and subtropical Atlantic, which can be attributed to an invigoration of modern-like AMOC (Tremblin et al., 2016; Elsworth et al., 2017; Vahlenkamp et al., 2018; Hutchinson et al., 2019; Toumoulin et al., 2020; Hutchinson et al., 2021). This inference is supported by the increasing meridional benthic foraminiferal $\delta^{18}O$ gradient among the Atlantic and Southern Oceans (Cramer et al., 2009) and enhanced vertical mixing between Atlantic intermediate and deep water inferred by the collapse in the planktic-benthic $\delta^{13}C$ gradient (Abelson and Erez, 2017; Coxall et al., 2018). The warming of SST in the Hiwannee core during the late Eocene indicates an increase in heat transport and supports the presence of a modern-like AMOC in the Atlantic, which would result in northward heat transport and a warmer Northern Hemisphere than Southern Hemisphere (Buckley and Marshall, 2016).

The TEX_{86} temperatures reported here agree with other temperature proxy data and benthic $\delta^{18}O$ records and reveal that the SST changes slightly across the EOT in the subtropics and Northern Hemisphere relative to >8 °C cooling in the Southern Hemisphere (Lear et al., 2008; Cramer et al., 2009; Liu et al., 2018). The magnitude of change in the SST at the Hiwannee core location is consistent with the $U^{K'}_{37}$ SST data from Site 1404 in the North Atlantic (Fig. 6B), where the SST decreases less than 2 °C in association with the EOT (Liu et al., 2018). In addition, terrestrial paleoclimatic proxy data from the Northern Hemisphere (Fig. 6A) also show a delayed cooling that does not begin until the EOGM at ca. 33.65 Ma (Zanazzi et al., 2007; Hren et al., 2013; Fan et al., 2017). For example, temperature proxy data from continental North America indicate that there is a more pronounced cooling (~7–8 °C) from the late Eocene into the early Oligocene, while the major phase of cooling occurs after ca. 33.6 Ma. Contrary to the Northern Hemisphere, the $U^{K'}_{37}$ SST from site 511 in the Southern Ocean (Fig. 6B) strikingly declines during the late Eocene, which is ~0.5–1 m.y. earlier than the cooling in the Northern Hemisphere (Liu et al., 2009). This asymmetric temperature pattern across the EOT is unlikely to be attributed to the $_pCO_2$ drop alone, which is supposed to synchronously cool global temperatures. Climate simulations and proxy data indicate that the southern–northern temperature difference is associated with the establishment of the Antarctic Ice Sheet, which intensifies the meridional temperature gradient and invigorates oceanic circulation (Goldner et al., 2014; Liu et al., 2018). A recent modeling study proposes another hypothesis that illustrates the effect of the closure of the Arctic–Atlantic gateway, which suggests that a strengthened AMOC, due to closure of the seaway, might increase oceanic carbon uptake, enhance weathering, and in turn cause a reduction of atmospheric CO_2 and Antarctic glaciation (Hutchinson et al., 2019).

Hydrological Changes in the Gulf of Mexico Driven by Interhemispherically Asymmetric Temperatures

An increase in precipitation is synchronous with a positive shift in global marine $\delta^{18}O$ records (Cramer et al., 2009), and a cooling of southern high-latitude temperatures (Liu et al., 2009; Figs. 6B–6D), which indicates that the hydrological change along the Gulf Coast is associated with changes in meridional temperature gradients and the reorganization of oceanic and atmospheric circulation. Here it is argued that

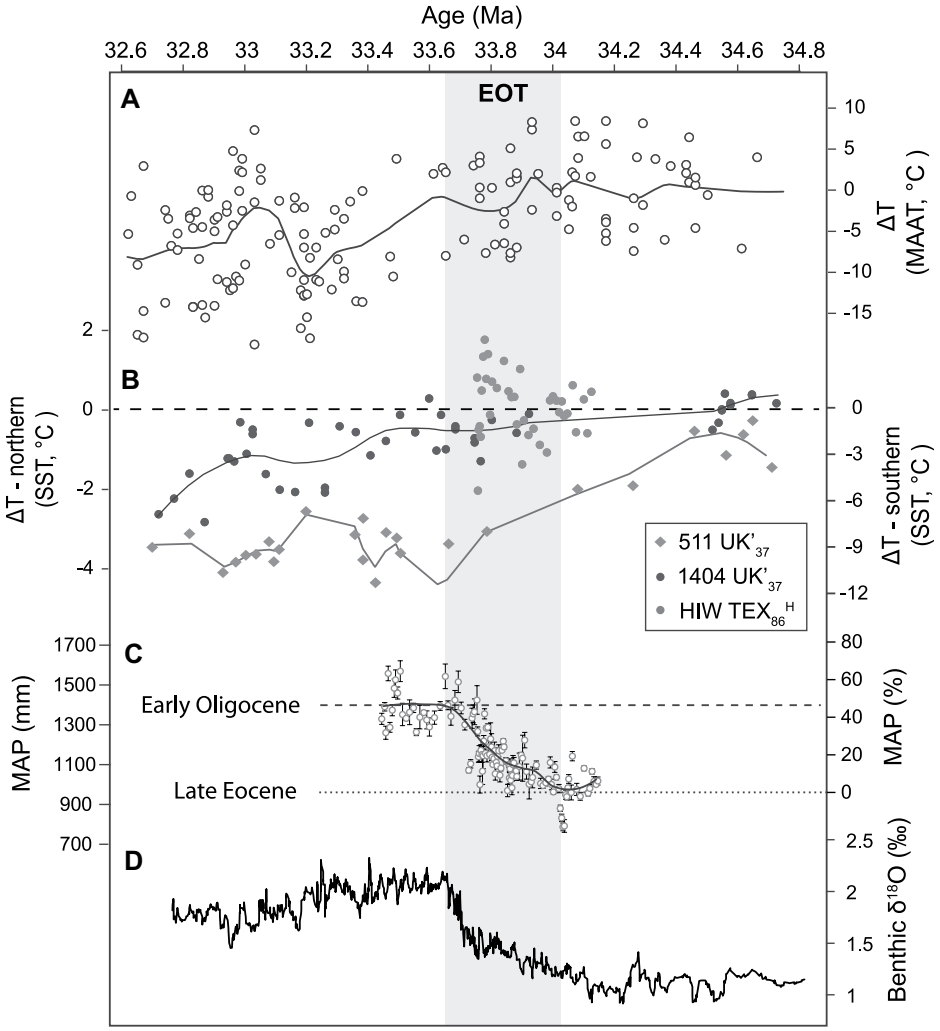

Figure 6. Comparison of leaf wax isotope-based rainfall variations and temperature records in both hemispheres is shown. (A) Change in mean annual average temperature (MAAT) from continental records (Zanazzi et al., 2007; Hren et al., 2013; Fan et al., 2017); data are smoothed by local regression (curves). (B) Sea-surface temperatures (SST) from sites 511 (North Atlantic) and 1404 (South Atlantic) (Plancq et al., 2014; Liu et al., 2018) and new TEX_{86} at Hiwannee (Gulf of Mexico). Temperature changes (ΔT) are relative to the mean values between 34.5 Ma and 37 Ma at individual localities. SSTs in sites 511 and 1404 (points) are smoothed by local regression (curves). (C) Reconstructed mean annual precipitation (MAP) based on $\delta^{13}C_{wax}$; dashed line represents the average MAP for the early Oligocene (33.45–33.70 Ma); dotted line denotes the average MAP for the late Eocene (before 34.0 Ma). Change of MAP in percentage (MAP%) is calculated relative to the mean values for the late Eocene (before 34.0 Ma) and is reported in percent (%). The shaded bar denotes the Eocene–Oligocene transition (EOT) interval. (D) Global benthic $\delta^{18}O$ records with a 10-point moving average (Cramer et al., 2009).

increased precipitation across the EOT is associated with a strengthened AMOC that shifts the Intertropical Convergence Zone northward. Millennial-scale climatic modeling for glacial–interglacial cycles has suggested that the interhemispheric asymmetric temperature gradient impacts the Hadley and eddy circulation and forces the Intertropical Convergence Zone to shift toward relatively warmer regions by alternating atmospheric heat exchange between the tropics and mid-latitudes (Broccoli et al., 2006; Chiang and Friedman, 2012). Substantial cooling in the Southern Hemisphere and AMOC-intensifying northward heat transport across the EOT would be expected to strengthen the southern Hadley cell and weaken the northern Hadley cell, which enlarges the meridional pressure gradient between the Southern and Northern Hemisphere. This interhemispheric pressure gradient potentially enhances moisture and heat transport from the subtropical Atlantic to the Gulf Coast, shifting the Intertropical Convergence Zone toward the relatively warmer Northern Hemisphere with intensified rainfall in Gulf of Mexico regions. Similar interhemispheric climate dynamics driven by Intertropical Convergence Zone displacement have also been proposed to explain the Quaternary climatic change in the Gulf of Mexico (Suh et al., 2020) and East Asian summer monsoon intensification during the late Miocene–Pliocene (Ao et al., 2016) and middle Miocene (Holbourn et al., 2010).

The northward migration of the Intertropical Convergence Zone is supported by a dust provenance study from central equatorial Pacific site 1334 that suggests a northward shift of the rain belt across the EOT (Hyeong et al., 2016). However, precipitation remains unchanged or decreases in the mid- to high latitudes in North America (Sheldon and Retallack, 2004; Retallack, 2007; Zanazzi et al., 2007; Fan et al., 2017) and in mid-latitude Asia, including the Xining Basin (Dupont-Nivet et al., 2007) and Lanzhou Basin (Ao et al., 2020). In combination with these published studies, our study reveals that the enhanced precipitation due to the northward shift of the Intertropical Convergence Zone dominates the tropics and sub-tropics. This pattern broadly supports the results from climate modeling studies, which show enhanced precipitation predominantly in the low latitudes of the Northern Hemisphere (Elsworth et al., 2017). But our records also reveal differences in predictions of slightly strengthened precipitation in the Gulf of Mexico from modeling studies, which calls for extensive proxy studies and the incorporation of numerical modeling. Furthermore, the displacement of the Intertropical Convergence Zone appears to have produced a rapid change within 500 k.y., which is identical to the transient nature of interhemispherically asymmetric temperature patterns (Liu et al., 2018; Fig. 6).

CONCLUSIONS

Leaf wax carbon and hydrogen isotopic records indicate enhanced precipitation in the subtropical North American Gulf Coast region during the Eocene–Oligocene transition (34.1–33.6 Ma). Precipitation reconstruction from leaf wax carbon isotopic values suggests an increase in mean annual precipitation of 44%. The change in precipitation is accompanied by a secular increase in TEX_{86}-based sea-surface temperature reconstruction of ~2 °C during the latest Eocene. The enhanced precipitation in the Gulf of Mexico is attributed to the northward shift of the Intertropical Convergence Zone,

which was driven by the enlarged polar-tropic temperature gradient in the Southern Hemisphere and the strengthened Atlantic Meridional Overturning Circulation (AMOC). Paleoclimatic reconstruction supports the change in Atlantic Ocean circulation and the invigoration of modern-like AMOC during the late Eocene. These findings highlight the critical role of meridional temperature gradient and large-scale oceanic circulation in modulating tropical and subtropical hydroclimate and its potential impacts on CO_2-weathering feedback during the "greenhouse" to "icehouse" transition through the Eocene–Oligocene boundary.

ACKNOWLEDGMENTS

We thank the *GSA Bulletin* editor, associate editor, and anonymous reviewers for thorough and constructive comments that significantly improved the quality of the paper. We thank Zhonghui Liu and Feng Cheng for very helpful discussions and Hui Yang and Clay Doremus for their assistance in the laboratory. We acknowledge financial support from U.S. National Science Foundation Grant EAR 2022282 (to G. Zhuang).

REFERENCES CITED

Abelson, M., and Erez, J., 2017, The onset of modern-like Atlantic meridional overturning circulation at the Eocene–Oligocene transition: Evidence, causes, and possible implications for global cooling: Geochemistry, Geophysics, Geosystems, v. 18, no. 6, p. 2177–2199, https://doi.org/10.1002/2017GC006826.

Ao, H., Roberts, A.P., Dekkers, M.J., Liu, X., Rohling, E.J., Shi, Z., An, Z., and Zhao, X., 2016, Late Miocene–Pliocene Asian monsoon intensification linked to Antarctic ice-sheet growth: Earth and Planetary Science Letters, v. 444, p. 75–87, https://doi.org/10.1016/j.epsl.2016.03.028.

Ao, H., Dupont-Nivet, G., Rohling, E.J., Zhang, P., Ladant, J.B., Roberts, A.P., Licht, A., Liu, Q., Liu, Z., Dekkers, M.J., Coxall, H.K., Jin, Z., Huang, C., Xiao, G., Poulsen, C.J., Barbolini, N., Meijer, N., Sun, Q., Qiang, X., Yao, J., and An, Z., 2020, Orbital climate variability on the northeastern Tibetan Plateau across the Eocene–Oligocene transition: Nature Communications, v. 11, no. 1, 5249, https://doi.org/10.1038/s41467-020-18824-8.

Borrelli, C., Cramer, B.S., and Katz, M.E., 2014, Bipolar Atlantic deepwater circulation in the middle–late Eocene: Effects of Southern Ocean gateway openings: Paleoceanography and Paleoclimatology, v. 29, no. 4, p. 308–327, https://doi.org/10.1002/2012PA002444.

Broccoli, A.J., Dahl, K.A., and Stouffer, R.J., 2006, Response of the Intertropical Convergence Zone to Northern Hemisphere cooling: Geophysical Research Letters, v. 33, no. 1, https://doi.org/10.1029/2005GL024546.

Buckley, M.W., and Marshall, J., 2016, Observations, inferences, and mechanisms of the Atlantic Meridional Overturning Circulation: A review: Reviews of Geophysics, v. 54, no. 1, p. 5–63, https://doi.org/10.1002/2015RG000493.

Bush, R.T., and McInerney, F.A., 2013, Leaf wax n-alkane distributions in and across modern plants: Implications for paleoecology and chemotaxonomy: Geochimica et Cosmochimica Acta, v. 117, p. 161–179, https://doi.org/10.1016/j.gca.2013.04.016.

Chiang, J.C.H., and Friedman, A.R., 2012, Extratropical cooling, interhemispheric thermal gradients, and tropical climate change: Annual Review of Earth and Planetary Sciences, v. 40, no. 1, p. 383–412, https://doi.org/10.1146/annurev-earth-042711-105545.

Coxall, H.K., Wilson, P.A., Palike, H., Lear, C.H., and Backman, J., 2005, Rapid stepwise onset of Antarctic glaciation and deeper calcite compensation in the Pacific Ocean: Nature, v. 433, no. 7021, p. 53–57, https://doi.org/10.1038/nature03135.

Coxall, H.K., Huck, C.E., Huber, M., Lear, C.H., Legarda-Lisarri, A., O'Regan, M., Sliwinska, K.K., van de Flierdt, T., de Boer, A.M., Zachos, J.C., and Backman, J., 2018, Export of nutrient rich Northern Component Water preceded early Oligocene Antarctic glaciation: Nature Geoscience, v. 11, no. 3, p. 190, https://doi.org/10.1038/s41561-018-0069-9.

Cramer, B.S., Toggweiler, J.R., Wright, J.D., Katz, M.E., and Miller, K.G., 2009, Ocean overturning since the Late Cretaceous: Inferences from a new benthic foraminiferal isotope compilation: Paleoceanography and Paleoclimatology, v. 24, https://doi.org/10.1029/2008PA001683.

DeConto, R.M., Pollard, D., Wilson, P.A., Palike, H., Lear, C.H., and Pagani, M., 2008, Thresholds for Cenozoic bipolar glaciation: Nature, v. 455, no. 7213, p. 652–656, https://doi.org/10.1038/nature07337.

Diefendorf, A.F., and Freimuth, E.J., 2017, Extracting the most from terrestrial plant-derived n-alkyl lipids and their carbon isotopes from the sedimentary record: A review: Organic Geochemistry, v. 103, p. 1–21, https://doi.org/10.1016/j.orggeochem.2016.10.016.

Diefendorf, A.F., Mueller, K.E., Wing, S.L., Koch, P.L., and Freeman, K.H., 2010, Global patterns in leaf ^{13}C discrimination and implications for studies of past and future climate: Proceedings of the National Academy of Sciences of the United States of America, v. 107, no. 13, p. 5738–5743, https://doi.org/10.1073/pnas.0910513107.

Diefendorf, A.F., Freeman, K.H., Wing, S.L., and Graham, H.V., 2011, Production of n-alkyl lipids in living plants and implications for the geologic past: Geochimica et Cosmochimica Acta, v. 75, no. 23, p. 7472–7485, https://doi.org/10.1016/j.gca.2011.09.028.

Dupont-Nivet, G., Krijgsman, W., Langereis, C.G., Abels, H.A., Dai, S., and Fang, X., 2007, Tibetan plateau aridification linked to global cooling at the Eocene–Oligocene transition: Nature, v. 445, no. 7128, p. 635–638, https://doi.org/10.1038/nature05516.

Eglinton, G., and Hamilton, R.J., 1967, Leaf epicuticular waxes: Science, v. 156, no. 3780, p. 1322, https://doi.org/10.1126/science.156.3780.1322.

Ehleringer, J.R., Phillips, S.L., Schuster, W.S.F., and Sandquist, D.R., 1991, Differential utilization of summer rains by desert plants: Oecologia, v. 88, no. 3, p. 430–434, https://doi.org/10.1007/BF00317589.

Ellwood, B.B., Febo, L., Anderson, L., Hackworth, R.T., Means, G.H., Bryan, J.A., Tomkin, J., Rowe, H., and Jovane, L., 2019, Regional to global correlation of Eocene–Oligocene boundary transition successions using biostratigraphic, geophysical and geochemical methods: Geological Magazine, v. 157, no. 1, p. 80–100, https://doi.org/10.1017/S0016756819000578.

Elsworth, G., Galbraith, E., Halverson, G., and Yang, S., 2017, Enhanced weathering and CO_2 drawdown caused by latest Eocene strengthening of the Atlantic meridional overturning circulation: Nature Geoscience, v. 10, no. 3, p. 213, https://doi.org/10.1038/ngeo2888.

Fan, M., Ayyash, S.A., Tripati, A., Passey, B.H., and Griffith, E.M., 2017, Terrestrial cooling and changes in hydroclimate in the continental interior of the United States across the Eocene–Oligocene boundary: Geological Society of America Bulletin, v. 130, no. 7–8, p. 1073–1084.

Farquhar, G.D., O'Leary, M.H., and Berry, J.A., 1982, On the relationship between carbon isotope discrimination and the intercellular carbon dioxide concentration in leaves: Functional Plant Biology, v. 9, no. 2, p. 121–137, https://doi.org/10.1071/PP9820121.

Ficken, K.J., Li, B., Swain, D., and Eglinton, G., 2000, An n-alkane proxy for the sedimentary input of submerged/floating freshwater aquatic macrophytes: Organic Geochemistry, v. 31, no. 7, p. 745–749, https://doi.org/10.1016/S0146-6380(00)00081-4.

Goldner, A., Herold, N., and Huber, M., 2014, Antarctic glaciation caused ocean circulation changes at the Eocene–Oligocene transition: Nature, v. 511, no. 7511, p. 574, https://doi.org/10.1038/nature13597.

Holbourn, A., Kuhnt, W., Regenberg, M., Schulz, M., Mix, A., and Andersen, N., 2010, Does Antarctic glaciation force migration of the tropical rain belt?: Geology, v. 38, no. 9, p. 783–786, https://doi.org/10.1130/G31043.1.

Hou, J., D'Andrea, W.J., MacDonald, D., and Huang, Y., 2007, Hydrogen isotopic variability in leaf waxes among terrestrial and aquatic plants around Blood Pond, Massachusetts (USA): Organic Geochemistry, v. 38, no. 6, p. 977–984, https://doi.org/10.1016/j.orggeochem.2006.12.009.

Hou, J., D'Andrea, W.J., and Huang, Y., 2008, Can sedimentary leaf waxes record D/H ratios of continental precipitation? Field, model, and experimental assessments: Geochimica et Cosmochimica Acta, v. 72, no. 14, p. 3503–3517, https://doi.org/10.1016/j.gca.2008.04.030.

Houben, A.J.P., Quaijtaal, W., Wade, B.S., Schouten, S., and Brinkhuis, H., 2019, Quantitative organic-walled dinoflagellate cyst stratigraphy across the Eocene–Oligocene Transition in the Gulf of Mexico: A record of climate- and sea level change during the onset of Antarctic glaciation: Newsletters on Stratigraphy, v. 52, no. 2, p. 131–154, https://doi.org/10.1127/nos/2018/0455.

Hren, M.T., Sheldon, N.D., Grimes, S.T., Collinson, M.E., Hooker, J.J., Bugler, M., and Lohmann, K.C., 2013, Terrestrial cooling in Northern Europe during the Eocene–Oligocene transition: Proceedings of the National Academy of Sciences of the United States of America, v. 110, no. 19, p. 7562–7567, https://doi.org/10.1073/pnas.1210930110.

Hutchinson, D.K., Coxall, H.K., O'Regan, M., Nilsson, J., Caballero, R., and de Boer, A.M., 2019, Arctic closure as a trigger for Atlantic overturning at the Eocene–Oligocene Transition: Nature Communications, v. 10, no. 1, p. 1–9, https://doi.org/10.1038/s41467-019-11828-z.

Hutchinson, D.K., Coxall, H.K., Lunt, D.J., Steinthorsdottir, M., de Boer, A.M., Baatsen, M., von der Heydt, A., Huber, M., Kennedy-Asser, A.T., and Kunzmann, L., 2021, The Eocene–Oligocene transition: A review of marine and terrestrial proxy data, models and model–data comparisons: Climate of the Past, v. 17, no. 1, p. 269–315, https://doi.org/10.5194/cp-17-269-2021.

Hyeong, K., Kuroda, J., Seo, I., and Wilson, P.A., 2016, Response of the Pacific inter-tropical convergence zone to global cooling and initiation of Antarctic glaciation across the Eocene Oligocene Transition: Scientific Reports, v. 6, no. 30647, https://doi.org/10.1038/srep30647.

Katz, M.E., Miller, K.G., Wright, J.D., Wade, B.S., Browning, J.V., Cramer, B.S., and Rosenthal, Y., 2008, Stepwise transition from the Eocene greenhouse to the Oligocene icehouse: Nature Geoscience, v. 1, no. 5, p. 329–334, https://doi.org/10.1038/ngeo179.

Katz, M.E., Cramer, B.S., Toggweiler, J.R., Esmay, G., Liu, C., Miller, K.G., Rosenthal, Y., Wade, B.S., and Wright, J.D., 2011, Impact of Antarctic circumpolar current development on late Paleogene ocean structure: Science, v. 332, no. 6033, p. 1076–1079, https://doi.org/10.1126/science.1202122.

Katz, R.W., Parlange, M.B., and Tebaldi, C., 2003, Stochastic modeling of the effects of large-scale circulation on daily weather in the southeastern United States, *in* Mearns, L.O., ed., Issues in the Impacts of Climate Variability and Change on Agriculture: Cham, Switzerland, Springer, p. 189–216.

Kim, J.-H., van der Meer, J., Schouten, S., Helmke, P., Willmott, V., Sangiorgi, F., Koc, N., Hopmans, E.C., and Damste, J.S.S., 2010, New indices and calibrations derived from the distribution of crenarchaeal isoprenoid tetraether lipids: Implications for past sea surface temperature reconstructions: Geochimica et Cosmochimica Acta, v. 74, no. 16, p. 4639–4654, https://doi.org/10.1016/j.gca.2010.05.027.

Lambert, W.J., and Aharon, P., 2010, Oxygen and hydrogen isotopes of rainfall and dripwater at DeSoto Caverns (Alabama, USA): Key to understanding past variability of moisture transport from the Gulf of Mexico: Geochimica et Cosmochimica Acta, v. 74, no. 3, p. 846–861, https://doi.org/10.1016/j.gca.2009.10.043.

Lear, C.H., Bailey, T.R., Pearson, P.N., Coxall, H.K., and Rosenthal, Y., 2008, Cooling and ice growth across the Eocene-Oligocene transition: Geology, v. 36, no. 3, p. 251–254, https://doi.org/10.1130/G24584A.1.

Liu, X.-L., Russell, D.A., Bonfio, C., and Summons, R.E., 2019, Glycerol configurations of environmental GDGTs investigated using a selective ***sn***2 ether cleavage protocol: Organic Geochemistry, v. 128, p. 57–62, https://doi.org/10.1016/j.orggeochem.2018.12.003.

Liu, Z., Pagani, M., Zinniker, D., DeConto, R., Huber, M., Brinkhuis, H., Shah, S.R., Leckie, R.M., and Pearson, A., 2009, Global cooling during the Eocene–Oligocene climate transition: Science, v. 323, no. 5918, p. 1187–1190, https://doi.org/10.1126/science.1166368.

Liu, Z., He, Y., Jiang, Y., Wang, H., Liu, W., Bohaty, S.M., and Wilson, P.A., 2018, Transient temperature asymmetry between hemispheres in the Palaeogene Atlantic Ocean: Nature Geoscience, v. 11, no. 9, p. 656, https://doi.org/10.1038/s41561-018-0182-9.

Miller, K.G., Browning, J.V., Aubry, M.P., Wade, B.S., Katz, M.E., Kulpecz, A.A., and Wright, J.D., 2008, Eocene–Oligocene global climate and sea-level changes: St. Stephens Quarry, Alabama: Geological Society of America Bulletin, v. 120, no. 1–2, p. 34–53, https://doi.org/10.1130/B26105.1.

Mo, K.C., and Schemm, J.E., 2008, Relationships between ENSO and drought over the southeastern United States: Geophysical Research Letters, v. 35, no. 15, L15701, https://doi.org/10.1029/2008GL034656.

Oboh-Ikuenobe, F.E., and Jaramillo, C.A., 2003, Palynological Patterns in Uppermost Eocene to Lower Oligocene Sedimentary Rocks in the U.S. Gulf Coast, *in* From Greenhouse to Icehouse: The Marine Eocene-Oligocene Transition, Columbia University Press, p. 269–282.

Ogg, J.G., Ogg, G., and Gradstein, F.M., 2016, A Concise Geologic Time Scale: 2016: Amsterdam, Elsevier, 250 p.

Pagani, M., Huber, M., Liu, Z., Bohaty, S.M., Henderiks, J., Sijp, W., Krishnan, S., and DeConto, R.M., 2011, The role of carbon dioxide during the onset of Antarctic glaciation: Science, v. 334, no. 6060, p. 1261–1264, https://doi.org/10.1126/science.1203909.

Pearson, P.N., Foster, G.L., and Wade, B.S., 2009, Atmospheric carbon dioxide through the Eocene–Oligocene climate transition: Nature, v. 461, no. 7267, p. 1110–1113, https://doi.org/10.1038/nature08447.

Plancq, J., Mattioli, E., Pittet, B., Simon, L., and Grossi, V., 2014, Productivity and sea-surface temperature changes recorded during the late Eocene–early Oligocene at DSDP Site 511 (South Atlantic): Palaeogeography, Palaeoclimatology, Palaeoecology, v. 407, p. 34–44, https://doi.org/10.1016/j.palaeo.2014.04.016.

Retallack, G.J., 2007, Cenozoic Paleoclimate on land in North America: The Journal of Geology, v. 115, no. 3, p. 271–294, https://doi.org/10.1086/512753.

Rozanski, K., Araguás-Araguás, L., and Gonfiantini, R., 1993, Isotopic patterns in modern global precipitation, *in* Swart, P.K., Lohmann, K.L., McKenzie, J., and Savin, S., eds., Climate change in continental isotopic records: American Geophysical Union Geophysical Monograph, v. 78, p. 1–37.

Sachse, D., Billault, I., Bowen, G.J., Chikaraishi, Y., Dawson, T.E., Feakins, S.J., Freeman, K.H., Magill, C.R., McInerney, F.A., van der Meer, M.T.J., Polissar, P., Robins, R.J., Sachs, J.P., Schmidt, H.-L., Sessions, A.L., White, J.W.C., West, J.B., and Kahmen, A., 2012, Molecular paleohydrology: Interpreting the hydrogen-isotopic composition of lipid biomarkers from photosynthesizing organisms: Annual Review of Earth and Planetary Sciences, v. 40, no. 1, p. 221–249, https://doi.org/10.1146/annurev-earth-042711-105535.

Schouten, S., Hopmans, E.C., Schefuss, E., and Damste, J.S.S., 2002, Distributional variations in marine crenarchaeotal membrane lipids: A new tool for reconstructing ancient sea water temperatures?: Earth and Planetary Science Letters, v. 204, no. 1–2, p. 265–274, https://doi.org/10.1016/S0012-821X(02)00979-2.

Sheldon, N.D., and Retallack, G.J., 2004, Regional paleoprecipitation records from the late Eocene and Oligocene of North America: The Journal of Geology, v. 112, no. 4, p. 487–494, https://doi.org/10.1086/421076.

Sheldon, N.D., Grimes, S.T., Hooker, J.J., Collinson, M.E., Bugler, M.J., Hren, M.T., Price, G.D., and Sutton, P.A., 2016, Coupling of marine and continental oxygen isotope records during the Eocene–Oligocene transition: Geological Society of America Bulletin, v. 128, no. 3–4, p. 502–510, https://doi.org/10.1130/B31315.1.

Sijp, W.P., England, M.H., and Toggweiler, J.R., 2009, Effect of ocean gateway changes under greenhouse warmth: Journal of Climate, v. 22, no. 24, p. 6639–6652, https://doi.org/10.1175/2009JCLI3003.1.

Suh, Y.J., Diefendorf, A.F., Freimuth, E.J., and Hyun, S., 2020, Last interglacial (MIS 5e) and Holocene paleohydrology and paleovegetation of midcontinental North America from Gulf of Mexico sediments: Quaternary Science Reviews, v. 227, https://doi.org/10.1016/j.quascirev.2019.106066.

Tierney, J.E., and Tingley, M.P., 2014, A Bayesian, spatially-varying calibration model for the TEX86 proxy: Geochimica et Cosmochimica Acta, v. 127, p. 83–106, https://doi.org/10.1016/j.gca.2013.11.026.

Tipple, B.J., and Pagani, M., 2010, A 35 Myr North American leaf-wax compound-specific carbon and hydrogen isotope record: Implications for C_4 grasslands and hydrologic cycle dynamics: Earth and Planetary Science Letters, v. 299, no. 1, p. 250–262, https://doi.org/10.1016/j.epsl.2010.09.006.

Tipple, B.J., Meyers, S.R., and Pagani, M., 2010, Carbon isotope ratio of Cenozoic CO_2: A comparative evaluation of available geochemical proxies: Paleoceanography and Paleoclimatology, v. 25, no. 3, https://doi.org/10.1029/2009PA001851.

Toggweiler, J., and Samuels, B., 1995, Effect of Drake Passage on the global thermohaline circulation: Deep-Sea Research. Part I, Oceanographic Research Papers, v. 42, no. 4, p. 477–500, https://doi.org/10.1016/0967-0637(95)00012-U.

Toumoulin, A., Donnadieu, Y., Ladant, J.B., Batenburg, S.J., Poblete, F., and Dupont-Nivet, G., 2020, Quantifying the effect of the Drake Passage opening on the Eocene Ocean: Paleoceanography and Paleoclimatology, v. 35, no. 8, https://doi.org/10.1029/2020PA003889.

Tremblin, M., Hermoso, M., and Minoletti, F., 2016, Equatorial heat accumulation as a long-term trigger of permanent Antarctic ice sheets during the Cenozoic: Proceedings of the National Academy of Sciences of the United States of America, v. 113, no. 42, p. 11782–11787, https://doi.org/10.1073/pnas.1608100113.

Vachon, R.W., Welker, J.M., White, J.W.C., and Vaughn, B.H., 2010, Monthly precipitation isoscapes ($\delta^{18}O$) of the United States: Connections with surface temperatures, moisture source conditions, and air mass trajectories: Journal of Geophysical Research: Atmospheres, v. 115, no. D21, https://doi.org/10.1029/2010JD014105.

Vahlenkamp, M., Niezgodzki, I., De Vleeschouwer, D., Lohmann, G., Bickert, T., and Paelike, H., 2018, Ocean and climate response to North Atlantic seaway changes at the onset of long-term Eocene cooling: Earth and Planetary Science Letters, v. 498, p. 185–195, https://doi.org/10.1016/j.epsl.2018.06.031.

Wade, B.S., and Pearson, P.N., 2008, Planktonic foraminiferal turnover, diversity fluctuations and geochemical signals across the Eocene/Oligocene boundary in Tanzania: Marine Micropaleontology, v. 68, no. 3–4, p. 244–255, https://doi.org/10.1016/j.marmicro.2008.04.002.

Wade, B.S., Houben, A.J.P., Quaijtaal, W., Schouten, S., Rosenthal, Y., Miller, K.G., Katz, M.E., Wright, J.D., and Brinkhuis, H., 2012, Multiproxy record of abrupt sea-surface cooling across the Eocene–Oligocene transition in the Gulf of Mexico: Geology, v. 40, no. 2, p. 159–162, https://doi.org/10.1130/G32577.1.

Wang, C.Z., and Enfield, D.B., 2001, The tropical Western Hemisphere warm pool: Geophysical Research Letters, v. 28, no. 8, p. 1635–1638, https://doi.org/10.1029/2000GL011763.

Zanazzi, A., Kohn, M.J., MacFadden, B.J., and Terry, D.O., Jr., 2007, Large temperature drop across the Eocene–Oligocene transition in central North America: Nature, v. 445, no. 7128, p. 639–642, https://doi.org/10.1038/nature05551.

Science Editor: Brad S. Singer
Associate Editor: Rupsa Roy

Manuscript Received 26 February 2021
Revised Manuscript Received 4 October 2021
Manuscript Accepted 3 November 2021

Printed in the USA